Suppression of strain coupling in perovskite $La_{0.6}Sr_{0.1}TiO_3$ by cation disorder

Christopher J. Howard and Zhaoming Zhang

Australian Nuclear Science and Technology Organization, Private Mail Bag 1, Menai, New South Wales 2234, Australia

Michael A. Carpenter

Department of Earth Sciences, University of Cambridge, Downing Street, Cambridge CB2 3EQ, United Kingdom

Kevin S. Knight

ISIS Facility, Rutherford Appleton Laboratory, Chilton, Didcot, Oxfordshire OX11 0QX, United Kingdom

An octahedral tilting transition has been investigated in two samples of $La_{0.6}Sr_{0.1}TiO_3$ by powder neutron diffraction. One (slowly cooled) sample had a degree of cation/vacancy ordering on the *A* sites and was tetragonal, $P4/mmm$, at high temperatures. The second (quenched) sample had disordered cations and cubic, $Pm\bar{3}m$, symmetry at high temperatures. On cooling, both underwent the same *R*-point tilting transition at $\sim 560-570$ K, to give symmetry changes $P4/mmm \leftrightarrow Cmmm$ and $Pm\bar{3}m \leftrightarrow I4/mcm$, respectively. From the evolution of the tilt angles, the transition appears to be close to tricritical in both cases. As expected from a Landau expansion in the two order parameters, the transition temperature was found to be only weakly dependent on the degree of cation order. In contrast with the expectation of standard patterns of strain to order parameter coupling, however, the tilted (tetragonal) form of the disordered sample remained metrically cubic, implying that coupling of the tetragonal shear strain with the octahedral tilting was suppressed. It is proposed that cation disordering causes the development of local strain heterogeneities in crystals of $La_{0.6}Sr_{0.1}TiO_3$ which prevent a coherent, long-range shear strain from developing. Manipulation of the degree of cation order in perovskites with carefully selected compositions might therefore provide a means by which the magnitudes of ferroelastic strains could be engineered according to the requirement of particular applications.

INTRODUCTION

Multiple phase transitions in a single material can, in principle, give rise to the development or modification of more than one distinct property of technological interest. In this context, the current search for "multiferroic" materials[1,2] is motivated by a desire to be able to manipulate different combinations of properties simultaneously by the application of external fields. In one class of such materials, the relevant atomic scale mechanisms all occur on a short time scale such that the responses to an applied field occur more or less instantaneously. This includes properties that are associated with changes in electronic structure, small atomic displacements, and realignment of magnetic or electric dipoles. There is a second class of materials, however, in which the local processes operate on quite different time scales. Here a key mechanism is chemical diffusion, and possibilities arise for rather different styles of manipulation. For example, a particular atomic configuration might be adjusted by annealing at high temperatures and then preserved by quenching. The selected configuration can then be used to control the development of properties associated with some more rapid transition at lower temperatures. This effect is well known in minerals such as albite $(NaAlSi_3O_8)$ and anorthite $(CaAl_2Si_2O_8)$, where changes in Al/Si ordering among crystallographic sites induced at high temperatures can have a significant influence on subsequent displacive phase transitions.[3–7] The effect is also known in ferroelectric materials where cation disordering can cause the ferroelectric transition to become diffuse.[8–10] The same concept does not seem

to have been applied to ferroelastic transitions in perovskites, however, and the purpose of the present paper is to describe an octahedral tilting transition for which the ferroelastic response displays a strong and unexpected sensitivity to ordering of cations and vacancies on *A* sites of the perovskite structure.

The work reported here follows our previous structural studies[11–13] of *A*-site-deficient perovskites with compositions close to $La_{2/3}TiO_3$. These perovskites, when prepared by slow cooling, show an ordering of cations and vacancies onto alternate planes such that the *A* sites in one plane are essentially fully occupied and those on the next only about one-third occupied. The structures also show a tilting of the TiO_6 octahedra at room temperature that is removed via a continuous phase transition as the temperature is raised. It became evident that, by varying the preparation, in particular by rapid cooling, the development of cation ordering could be largely prevented. The objectives of this work were to examine the spontaneous strain behavior of these otherwise identical perovskites at different degrees of cation ordering, focusing in particular on how cation ordering impacts on the octahedral tilting transition and how it modifies the ferroelastic response.

LANDAU THEORY

The perovskite structures formed by combining layered ordering on the *A* sites with in-phase $(+)$ and out-of-phase $(-)$ BX_6 octahedral tilting have been enumerated by Howard and Zhang.[12] The layered ordering of cations (or vacancies)

on the perovskite A site was recognized as transforming with the symmetry of the irreducible representation [irrep (Ref. 14)] X_3^- ($k=0,0,1/2$) of the aristotype $Pm\bar{3}m$ space group. As always,[15] the in-phase and out-of-phase octahedral tilting were taken to be associated with irreps M_3^+ ($k=1/2,1/2,0$) and R_4^+ ($k=1/2,1/2,1/2$), respectively.

For the compound actually studied in this work, $La_{0.6}Sr_{0.1}TiO_3$, the octahedral tilting has been found to be out-of-phase, R_4^+, tilting only. A master Landau free-energy expansion has therefore been constructed, using the computer program ISOTROPY,[16] to include order parameters associated with irreps X_3^- and R_4^+:

$$G = \frac{1}{2}a_1\Theta_{s1}\left[\coth\left(\frac{\Theta_{s1}}{T}\right) - \coth\left(\frac{\Theta_{s1}}{T_{c1}}\right)\right](q_1^2 + q_2^2 + q_3^2) + \frac{1}{2}a_2\Theta_{s2}\left[\coth\left(\frac{\Theta_{s2}}{T}\right) - \coth\left(\frac{\Theta_{s2}}{T_{c2}}\right)\right](q_4^2 + q_5^2 + q_6^2) + \frac{1}{4}b_1(q_1^2 + q_2^2 + q_3^2)^2$$

$$+ \frac{1}{4}b_1'(q_1^4 + q_2^4 + q_3^4) + \frac{1}{4}b_2(q_4^2 + q_5^2 + q_6^2)^2 + \frac{1}{4}b_2'(q_4^4 + q_5^4 + q_6^4) + \frac{1}{6}c_1(q_1^2 + q_2^2 + q_3^2)^3 + \frac{1}{6}c_1'(q_1q_2q_3)^2$$

$$+ \frac{1}{6}c_1''(q_1^2 + q_2^2 + q_3^2)(q_1^4 + q_2^4 + q_3^4) + \frac{1}{6}c_2(q_4^2 + q_5^2 + q_6^2)^3 + \frac{1}{6}c_2'(q_4q_5q_6)^2 + \frac{1}{6}c_2''(q_4^2 + q_5^2 + q_6^2)(q_4^4 + q_5^4 + q_6^4)$$

$$+ \lambda_q(q_1^2 + q_2^2 + q_3^2)(q_4^2 + q_5^2 + q_6^2) + \lambda_q'(q_2^2q_4^2 + q_3^2q_5^2 + q_1^2q_6^2) + \lambda_1 e_a(q_1^2 + q_2^2 + q_3^2) + \lambda_2 e_a(q_4^2 + q_5^2 + q_6^2)$$

$$+ \lambda_3[\sqrt{3}e_o(q_3^2 - q_1^2) + e_t(2q_2^2 - q_1^2 - q_3^2)] + \lambda_4[\sqrt{3}e_o(q_5^2 - q_6^2) + e_t(2q_4^2 - q_5^2 - q_6^2)] + \lambda_5(e_4q_4q_6 + e_5q_4q_5 + e_6q_5q_6)$$

$$+ \lambda_6(q_1^2 + q_2^2 + q_3^2)(e_4^2 + e_5^2 + e_6^2) + \lambda_7(q_1^2e_6^2 + q_2^2e_4^2 + q_3^2e_5^2) + \frac{1}{4}(C_{11}^0 - C_{12}^0)(e_o^2 + e_t^2) + \frac{1}{6}(C_{11}^0 + 2C_{12}^0)e_a^2 + \frac{1}{2}C_{44}^0(e_4^2 + e_5^2 + e_6^2).$$

(1)

Here q_1, q_2, and q_3 are components of the order parameter for cation (or vacancy) layered ordering. They correspond to ordering of cations onto planes perpendicular to the crystallographic y, z, and x axes, respectively, of the parent $Pm\bar{3}m$ perovskite [where these x, y, and z axes are aligned parallel to the reference axes X, Y, and Z of Eq. (1)]. The quantities q_4, q_5, and q_6 are components of the order parameter for tilting—they can be considered to correspond to tilts of the TiO_6 octahedra around the Z, X, and Y reference axes, respectively. Note that this free-energy expression is closely similar to that obtained for in-phase (M_3^+) and out-of-phase (R_4^+) tilts acting together.[17] The only difference is that the components q_1, q_2, and q_3 representing M_3^+ tilting have been cycled, being replaced here by q_2, q_3, and q_1, respectively. The quantities a_1, a_2, b_1, etc., are normal Landau coefficients, Θ_{s1} and Θ_{s2} are saturation temperatures, T_{c1} and T_{c2} are critical temperatures for the cation ordering and tilting transitions, respectively, λ_1, λ_q, etc., are coupling coefficients, C_{11}^0, C_{12}^0, and C_{44}^0 are bare elastic constants (i.e., of the parent cubic structure), and e_4, e_5, and e_6 are shear strain components. The symmetry-adapted strains e_a, e_o, and e_t are combinations of the linear strain components e_1, e_2, and e_3 as

$$e_a = (e_1 + e_2 + e_3),$$

(2)

$$e_o = (e_1 - e_2),$$

(3)

$$e_t = \frac{1}{\sqrt{3}}(2e_3 - e_1 - e_2).$$

(4)

To this point, only the lowest-order strain-order parameter coupling terms have been included. Direct biquadratic coupling, $\lambda_q q_1^2 q_4^2$, etc., is included for completeness although the coupling mechanism might be indirect via the common strain, in which case the direct coupling terms would not be required. Table I lists space groups for product structures described by this free-energy expansion for the $La_{0.6}Sr_{0.1}TiO_3$ system. Figure 1 shows the unit cells of these structures in relation to the cell of the parent $Pm\bar{3}m$ perovskite and the reference system of Eq. (1).

TABLE I. Properties of parent group $Pm\bar{3}m$ and selected subgroups derived by coupling between separate order parameter components associated with irreps X_3^- and R_4^+. The orientations are those indicated by computer program ISOTROPY.

	Order parameter components			
Subgroup	X_3^-	R_4^+	Lattice vectors	Origin
$Pm\bar{3}m$	0 0 0	0 0 0	(100),(010),(001)	(000)
$P4/mmm$	0 q_2 0	0 0 0	(100),(010),(002)	(00 1/2)
$I4/mcm$	0 0 0	0 q_5 0	(011),(0$\bar{1}$1),(200)	(000)
$Cmmm$	0 q_2 0	0 q_5 0	(200),(0$\bar{2}$0),(00$\bar{2}$)	(1 1/2 −1/2)
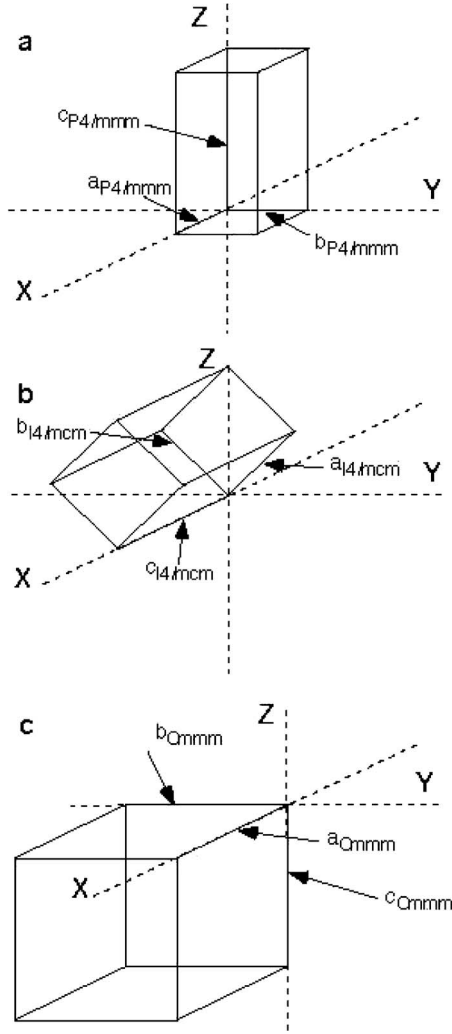
FIG. 1. Relationships between unit cell orientations for $P4/mmm$, $I4/mcm$, and $Cmmm$ structures derived from a $Pm\bar{3}m$ parent structure, as specified by Eq. (1) and Table I.

Since the only nonzero parameters in the structures we are considering are q_2 and q_5, the master Eq. (1) can be reduced to

$$
\begin{aligned}
G &= \frac{1}{2}a_1\Theta_{s1}\left[\coth\left(\frac{\Theta_{s1}}{T}\right) - \coth\left(\frac{\Theta_{s1}}{T_{c1}}\right)\right]q_2^2 \\
&+ \frac{1}{2}a_2\Theta_{s2}\left[\coth\left(\frac{\Theta_{s2}}{T}\right) - \coth\left(\frac{\Theta_{s2}}{T_{c2}}\right)\right]q_5^2 + \frac{1}{4}(b_1 + b_1')q_2^4 \\
&+ \frac{1}{4}(b_2 + b_2')q_5^4 + \frac{1}{6}(c_1 + c_1'')q_2^6 + \frac{1}{6}(c_2 + c_2'')q_5^6 + \lambda_q q_2^2 q_5^2 \\
&+ \lambda_1 e_a q_2^2 + \lambda_2 e_a q_5^2 + 2\lambda_3 e_t q_2^2 + \lambda_4\left[\sqrt{3}e_o q_5^2 - e_t q_5^2\right] \\
&+ \lambda_6 q_2^2(e_4^2 + e_5^2 + e_6^2) + \lambda_7 q_2^2 e_4^2 + \frac{1}{4}(C_{11}^0 - C_{12}^0)(e_o^2 + e_t^2) \\
&+ \frac{1}{6}(C_{11}^0 + 2C_{12}^0)e_a^2 + \frac{1}{2}C_{44}^0(e_4^2 + e_5^2 + e_6^2).
\end{aligned}
\tag{5}
$$

Applying the equilibrium conditions $\partial G/\partial e = 0$ leads to the following relationships between strains and order parameters:

$$
e_a = -\frac{(\lambda_1 q_2^2 + \lambda_2 q_5^2)}{\frac{1}{3}(C_{11}^0 + 2C_{12}^0)},
\tag{6}
$$

$$
e_t = \frac{\lambda_4 q_5^2 - 2\lambda_3 q_2^2}{\frac{1}{2}(C_{11}^0 - C_{12}^0)},
\tag{7}
$$

$$
e_o = \frac{-\lambda_4\sqrt{3}q_5^2}{\frac{1}{2}(C_{11}^0 - C_{12}^0)},
\tag{8}
$$

$$
e_4 = e_5 = e_6 = 0.
\tag{9}
$$

Substituting these into (5) gives

$$
\begin{aligned}
G &= \frac{1}{2}a_1\Theta_{s1}\left[\coth\left(\frac{\Theta_{s1}}{T}\right) - \coth\left(\frac{\Theta_{s1}}{T_{c1}}\right)\right]q_2^2 \\
&+ \frac{1}{2}a_2\Theta_{s2}\left[\coth\left(\frac{\Theta_{s2}}{T}\right) - \coth\left(\frac{\Theta_{s2}}{T_{c2}}\right)\right]q_5^2 + \frac{1}{4}b_1^* q_2^4 + \frac{1}{4}b_2^* q_5^4 \\
&+ \frac{1}{6}(c_1 + c_1'')q_2^6 + \frac{1}{6}(c_2 + c_2'')q_5^6 + \lambda_q^* q_2^2 q_5^2,
\end{aligned}
\tag{10}
$$

an expansion that incorporates the renormalized Landau and coupling coefficients as

$$
b_1^* = b_1 + b_1' - \frac{2\lambda_1^2}{\frac{1}{3}(C_{11}^0 + 2C_{12}^0)} - \frac{8\lambda_3^2}{\frac{1}{2}(C_{11}^0 - C_{12}^0)},
\tag{11}
$$

$$
b_2^* = b_2 + b_2' - \frac{2\lambda_2^2}{\frac{1}{3}(C_{11}^0 + 2C_{12}^0)} - \frac{8\lambda_4^2}{\frac{1}{2}(C_{11}^0 - C_{12}^0)},
\tag{12}
$$

$$
\lambda_q^* = \lambda_q - \frac{\lambda_1\lambda_2}{\frac{1}{3}(C_{11}^0 + 2C_{12}^0)} + \frac{2\lambda_3\lambda_4}{\frac{1}{2}(C_{11}^0 - C_{12}^0)}.
\tag{13}
$$

The situation considered in this paper is that in which the parameter q_2, corresponding to the state of cation order, is fixed at different values according to the sample preparation procedure and remains fixed over the temperature range in which the octahedral tilting order parameter q_5 is studied. Equation (10) then reads as a 2-4-6 expansion for the tilting order parameter q_5, and the equilibrium condition giving the value of this order parameter will be

$$
\begin{aligned}
\frac{\partial G}{\partial q_5} &= a_2\Theta_{s2}\left[\coth\left(\frac{\Theta_{s2}}{T}\right) - \coth\left(\frac{\Theta_{s2}}{T_{c2}}\right)\right]q_5 + b_2^* q_5^3 \\
&+ (c_2 + c_2'')q_5^5 + 2\lambda_q^* q_2^2 q_5 = 0.
\end{aligned}
\tag{14}
$$

For T, $T_{c2} \gg \Theta_{s2}$, $a_2\Theta_{s2}[\coth((\Theta_{s2}/T)) - \coth((\Theta_{s2}/T_{c2}))]$ be-

comes $a_2(T-T_{c2})$ and the renormalized transition temperature is given by

$$T_{c2}^* = T_{c2} - 2\lambda_q^* q_2^2/a_2. \tag{15}$$

If the transition is close to tricritical in character ($b_2^* \approx 0$), the result from Eq. (14) will be, again for T, $T_{c2} \gg \Theta_{s2}$,

$$q_5^4 = \frac{a_2(T_{c2}^* - T)}{c_2 + c_2''}. \tag{16}$$

For $La_{0.6}Sr_{0.1}TiO_3$, the relationships among T_{c1}, T_{c2}, Θ_{s1}, and Θ_{s2} are $T_{c1} > T_{c2} > \Theta_{s1}$, Θ_{s2}. The Landau description therefore leads to simple predictions of how the tilting transition should develop in crystals with different but fixed degrees of cation order. First, the effect of direct coupling through the biquadratic term, $\lambda_q q_2^2 q_5^2$ and indirect coupling through the common strains [Eq. (13)] should be for the tilting transition to occur at a different transition temperature according to the degree of cation order present [Eq. (15)]. Second, the tilting transition is expected to give rise to an orthorhombic strain e_o [Eq. (8)] and a change in the tetragonal strain e_t [Eq. (7)]. The excess tetragonal strain due to q_5^2 will be a factor of $\sqrt{3}$ smaller than e_o and have opposite sign. Finally, the evolution of the order parameter (effectively the octahedral tilt angle) below T_{c2}^* should be independent of q_2, since the fourth order coefficient b_2^* remains a constant [Eq. (12)]. What we observe experimentally, below, is that reducing q_2 leads to a substantial reduction in the magnitude of the tetragonal strain as well as causing a more subtle change in the evolution of the tilt angle. This can be understood if the coupling coefficient λ_4 is itself sensitive to q_2 in a manner not anticipated in Eq. (1).

EXPERIMENT

Sample preparation

The $La_{0.6}Sr_{0.1}TiO_3$ samples were produced by a standard alkoxide-nitrate route,[18] wherein stoichiometric quantities of ethanolic titanium isopropoxide were hydrolyzed by mixed lanthanum and strontium nitrate aqueous solutions. After thorough mixing and stir drying, the materials were calcined in air for 1 h to remove nitrates and alcohol, then subjected to 16 h of wet milling using zirconia balls. The slurry was dried overnight at 110 °C, and then the dried clumps were crushed in a mortar and pestle into fine powder. This powder was pelletized prior to subsequent heat treatment.

The heat treatments were varied to produce samples with two different degrees of cation and vacancy order. The "slowly cooled" sample (one 10 g pellet) was sintered in air at 1500 °C for 48 h, followed by a slow cooling process to promote the cation and vacancy ordering (5 °C/min to 1100 °C, then 0.05 °C/min from 1100 to 500 °C, and finally furnace cooled to room temperature). The "quenched" sample (ten 1 g pellets) was first sintered in air at 1400 °C for 96 h and furnace cooled to room temperature, followed by a subsequent quenching process from 1350 °C (comprising 2 h at 1350 °C before being quenched to room temperature). The quenching here was intended to preserve the disorder as presumed to exist at 1350 °C.

Both types of samples were characterized by scanning electron microscopy, using a JEOL 6400 instrument fitted with a Tracor Northern energy dispersive spectrometer operated at 15 kV. A comprehensive set of standards was used for quantitative work, giving a high degree of accuracy. This verified the sample composition and showed the samples to be homogeneous, with very small amounts of rutile ($<1\%$, just detectable in the diffraction patterns) in the slowly cooled sample and of $La_4Ti_9O_{24}$ ($<1\%$, not detectable by diffraction) in the quenched one. Finally, both samples were crushed to fine powder using a mortar and pestle for neutron powder diffraction.

Neutron diffraction

Time-of-flight powder neutron diffraction data were recorded using the high-resolution powder diffractometer (HRPD) at the ISIS neutron facility, Rutherford Appleton Laboratories, UK.[19] The two powdered samples—slow cooled and quenched—were loaded into thin-walled 11-mm-diameter vanadium sample cans. For room temperature measurement, the sample can was suspended in the vacuum tank from the standard ISIS candlestick. For the higher-temperature measurements an ISIS-designed furnace was used. This furnace employs a cylindrical vanadium element and operates under high vacuum (pressure $<10^{-4}$ mbar). The thermometry is based on type K (Chromel-Alumel) thermocouples positioned in contact with the sample about 20 mm above the beam center. The diffraction patterns were recorded in both back-scattering and 90° detector banks, over the time-of-flight range 30–130 ms, corresponding to d spacings from 0.6 to 2.6 Å (at a resolution $\Delta d/d \sim 4 \times 10^{-4}$) and from 0.9 to 3.7 Å ($\Delta d/d \sim 2 \times 10^{-3}$), respectively. The patterns were normalized to the incident beam spectrum as recorded in the upstream monitor, and corrected for detector efficiency according to prior calibration with a vanadium scan. Room temperature patterns were recorded to a total incident proton beam in the range 35–40 μA h corresponding to a minimum 1 h of data collection, and the high-temperature patterns to a total incident proton beam of about 8 μA h, corresponding to roughly 15 min of data collection. The temperature intervals ranged from 25 down to 5 K in the vicinity of the octahedral tilting phase transition. Thermal equilibration was achieved by delaying data collection for a period of at least 5 min (depending on the size of the temperature step) after stability at the set temperature had been achieved.

Diffraction patterns and phase identification

Four different structures have been encountered in this work, the details of which have been recorded in Table I. We remark that $q_2 \neq 0$ will lead to the appearance of what we term X-point reflections, indexing with two even and one odd index when referred to a doubled perovskite cell, and that $q_5 \neq 0$ leads to R-point reflections with indices all odd.

The slowly cooled sample shows, as before,[11] both cation ordering ($q_2 \neq 0$) and octahedral tilting ($q_5 \neq 0$) at room temperature, hence its space group is *Cmmm*. The X-point re-
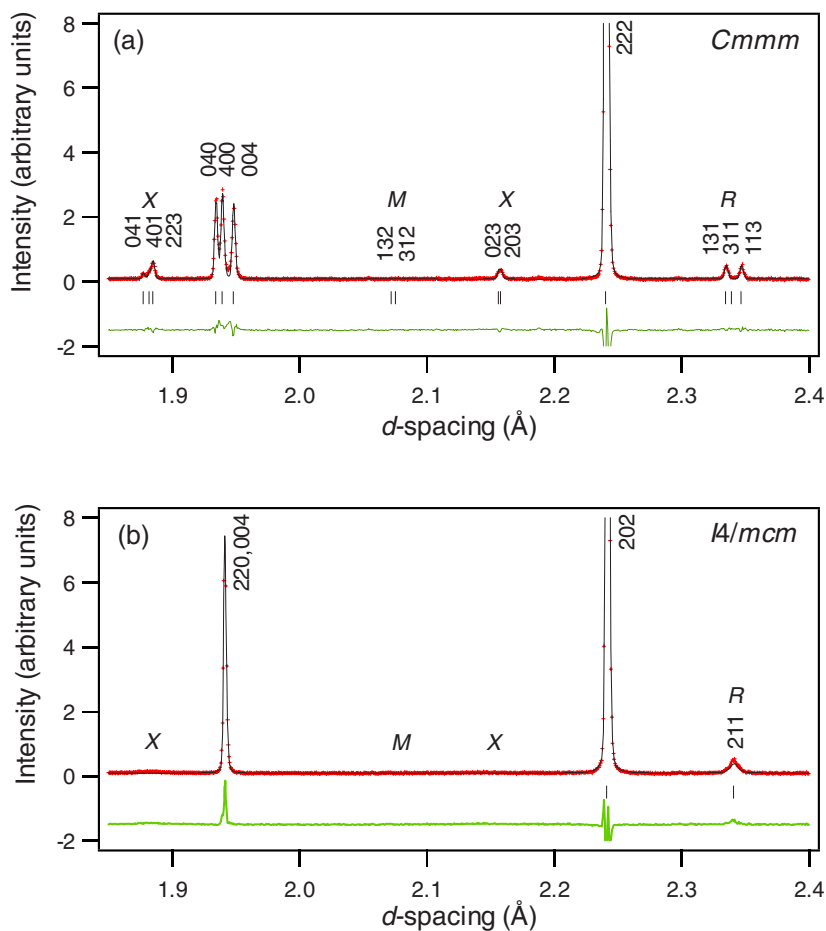
FIG. 2. (Color online) Extracts ($1.85 < d < 2.4$ Å) from the neutron diffraction patterns recorded in the back-scattering detector banks from (a) slowly cooled and (b) quenched $La_{0.6}Sr_{0.1}TiO_3$. The plots are the usual Rietveld method graphics, wherein crosses represent the observed data, continuous lines through these are the fitted patterns, vertical markers show the expected peak positions, and the line beneath the pattern records the difference between the observed pattern and that calculated in the Rietveld analysis. The peaks are indexed on cells of dimensions $2 \times 2 \times 2$ or $\sqrt{2} \times \sqrt{2} \times 2$ (referred to the edge of the cubic aristotype) as appropriate for the space group and structure assumed. In the pattern from the quenched sample, (b), the almost total absence of intensity around the X points confirms that in this sample the cation/vacancy ordering has been largely suppressed. For further discussion, see text.

flections, indicative of cation and vacancy ordering, as well as R-point reflections arising from the octahedral tilting, are both readily seen [Fig. 2(a)]. The combination of these two effects induces an orthorhombic distortion, evident through the resolved triplet at {004}.

The room temperature diffraction pattern from the quenched sample shows only trace diffuse intensity at the X points [Fig. 2(b)], confirming that cation ordering is largely suppressed ($q_2 = 0$). However, there remain significant, if broadened, peaks at the R points, attributed as usual to octahedral tilting ($q_5 \neq 0$). Accordingly, the space group is taken to be $I4/mcm$. The coincidence of the 220 and 004 peaks in this tetragonal structure indicates that this structure is metrically very nearly cubic.

Heating either sample leads to the removal, at around 280 °C, of octahedral tilting, evidenced by the disappearance of the R-point reflections. For the slowly cooled sample, this corresponds to a transition from the orthorhombic structure in $Cmmm$ ($q_2 \neq 0$, $q_5 \neq 0$) to the tetragonal in $P4/mmm$ ($q_2 \neq 0$, $q_5 = 0$). The disappearance of the R-point reflections, and the increase in symmetry from orthorhombic to tetragonal, are both seen through the diffraction data presented in Fig. 3. For the quenched sample, the transition is one from a metrically cubic $I4/mcm$ ($q_2 = 0$, $q_5 \neq 0$) to the cubic structure in $Pm\bar{3}m$ ($q_2 = q_5 = 0$).

Structure refinement

Phase identification was followed by structure refinement. In this, the neutron diffraction patterns were fitted, and both lattice parameters and atomic positions determined, using the Rietveld method[20] as implemented in the GSAS computer program.[21,22] Patterns from both the back-scattering and 90° detector banks were fitted simultaneously, the diffractometer constant for the 90° bank being refined once for each independent experimental setup and then fixed at the value so obtained. The peak shapes were modeled as convolutions of back-to-back exponentials with a pseudo-Voigt function and, for the back-scattering and 90° data, respectively, two and three peak width parameters were varied. The background was modeled as a sum of Chebyshev polynomials. The starting models for the structures in the slowly cooled sample, in space groups $Cmmm$ and $P4/mmm$, were taken from our earlier publication.[11] The starting models for the structures in the quenched sample were in space groups $I4/mcm$ and $Pm\bar{3}m$, as for standard ABX_3 perovskites in the same space groups, apart from reduced A-site occupancy. Internal coordinates were refined along with displacement parameters, the latter being taken to be isotropic except for the oxygen displacement parameter in the $Pm\bar{3}m$ structure which was taken to be anisotropic. Cation occupancies were set, not refined, in this work. In the slowly cooled sample the A sites in one layer were assumed to be fully occupied by La^{3+} ions, and

(a)

(b)
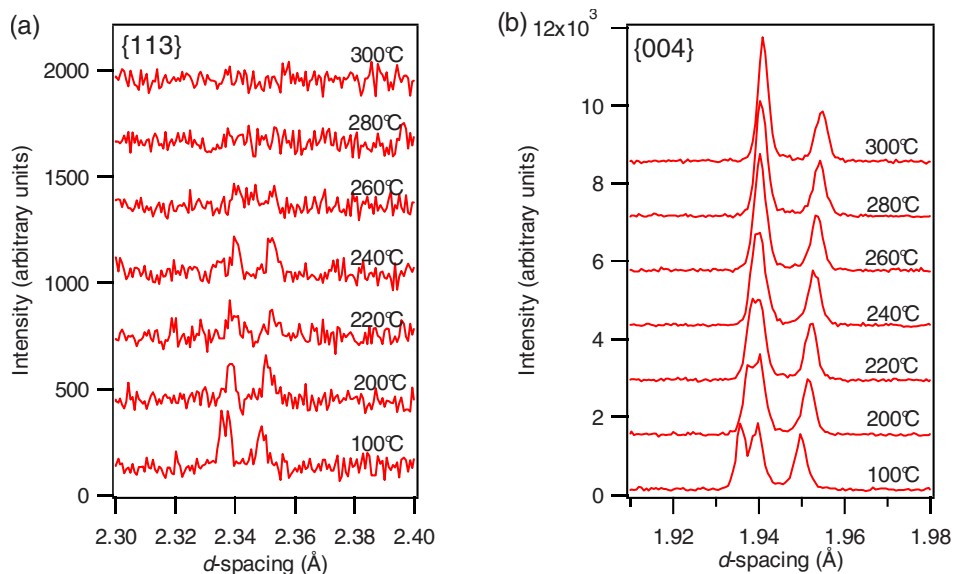
FIG. 3. (Color online) Extracts (a) $2.30 < d < 2.40$ Å and (b) $1.91 < d < 1.98$ Å from the neutron diffraction patterns recorded in the back-scattering detectors from slowly cooled $La_{0.6}Sr_{0.1}TiO_3$ at different temperatures. The intensities of the {113} R-point reflections diminish as the temperature is raised, while the symmetry as seen in the {004} set of reflections increases from orthorhombic to tetragonal.

the A sites in the next occupied 20% by La^{3+} and 20% by Sr^{2+}. (There are, along with limited experimental evidence,[11] theoretical grounds[23] for believing that the cation arrangement will be such as to maximize charge on the occupied layer.) In the quenched samples all A sites were considered to be 60% occupied by La^{3+} and 10% by Sr^{2+}.

The lattice parameters obtained from these refinements, suitably scaled for comparison with the cubic reference structure, are shown in Fig. 4. The orthorhombic to tetragonal transition in the slowly cooled sample is evident. The transition tetragonal to cubic in the quenched sample can be seen quite readily in the diffraction patterns (disappearance of R-point reflections), but is not evident in the metric. The scaled cell volume, that is, the volume per formula unit, is greater for the disordered cation arrangement (quenched sample) than for the ordered one irrespective of temperature, as might be expected,[23] but the difference is only about 0.15%. This difference will show as a volume strain in the analysis to follow.

Octahedral tilting ($q_5 \neq 0$) occurs in the orthorhombic $Cmmm$ and tetragonal $I4/mcm$ structures, and the tilt angle is estimated from the atomic coordinates. With the same atom labeling that appears in our previous publications[11,24] the tilt angle ϕ was estimated for the $I4/mcm$ structure from $\tan \phi = 1 - 4x(O2)$, and for the $Cmmm$ structure from $\tan \phi = 2[z(O4) - z(O3)]c/b$.

The evolution of the octahedral tilt angle ϕ for both quenched and slowly cooled samples is shown in Fig. 5(a). The tilting transition appears to be close to tricritical in character, since ϕ^4 varies approximately linearly with temperature for both samples [$q_5^4 \propto (T_{c2}^* - T)$; Fig. 5(b)]. The linear fits shown in Fig. 5(b) give $T_{c2}^* = 561$ and 571 K, respectively, for the slowly cooled and quenched samples. Slight differences in the slopes of these fits suggest that the evolution of tilt angle with temperature may be not quite the same in both samples.

STRAIN ANALYSIS

The linear strain components e_1, e_2, and e_3 have been calculated for the unit cell orientations shown in Fig. 1 as, for the $P4/mmm$ structure,

$$e_1 = e_2 = \frac{a - a_0}{a_0}, \quad e_3 = \frac{c/2 - a_0}{a_0}, \quad (17)$$

for the $Cmmm$ structure,

$$e_1 = \frac{a/2 - a_0}{a_0}, \quad e_2 = \frac{b/2 - a_0}{a_0}, \quad e_3 = \frac{c/2 - a_0}{a_0}, \quad (18)$$

and, for the $I4/mcm$ structure,
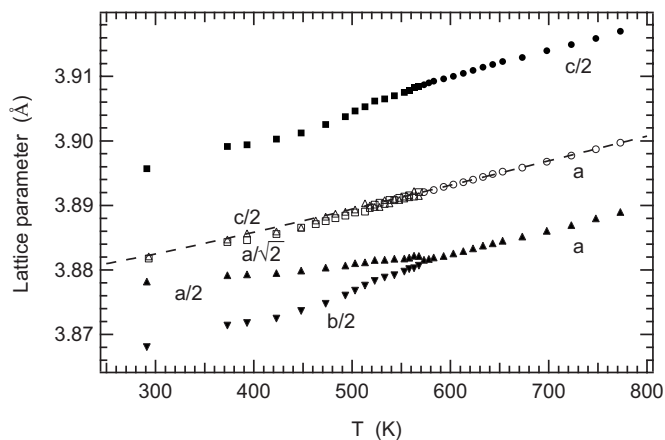
FIG. 4. Lattice parameter variations as a function of temperature for the slowly cooled (filled symbols) and quenched (open symbols) samples of $La_{0.6}Sr_{0.1}TiO_3$. The quantities plotted are a for the cubic phase, $c/2$ and $a/\sqrt{2}$ for the tetragonal structure in $I4/mcm$, $c/2$ and a for the tetragonal structure in $P4/mmm$, and $c/2$, $a/2$, and $b/2$ for the orthorhombic structure. The dashed line is a fit of Eq. (21) to data from the quenched sample for the temperature range in which it has cubic symmetry.
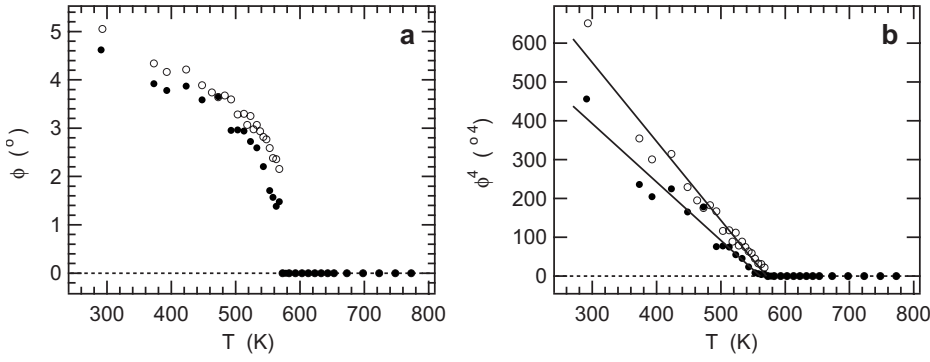
FIG. 5. Variation of the octahedral tilt angle ϕ with temperature for the slowly cooled (filled circles) and quenched (open circles) samples. Linear fits to the data for ϕ^4 against temperature suggest that the tilting transition is approximately tricritical in both samples.

$$e_1 = \frac{c/2 - a_0}{a_0}, \quad e_2 = e_3 = \frac{a/\sqrt{2} - a_0}{a_0}. \tag{19}$$

Here a_0 is the reference parameter for the $Pm\bar{3}m$ structure and a, b, and c are observed lattice parameters. The orientation of the relevant $I4/mcm$ cell has its unique axis aligned parallel to the reference X axis, and the tetragonal strain shown in Fig. 6 has been calculated as

$$e_{tx} = \frac{1}{\sqrt{3}}(2e_1 - e_2 - e_3) \quad \left(= \frac{1}{2}(\sqrt{3}e_o - e_t) \right). \tag{20}$$

The temperature dependence of a_0 must be such that it has zero slope as $T \to 0$ K. This can be effectively described by a function of the form[17,25–28]

$$a_0 = a_1 + a_2 \Theta_{s0} \coth\left(\frac{\Theta_{s0}}{T}\right), \tag{21}$$

where Θ_{s0} is the saturation temperature for the lattice parameter of the cubic structure. The experimental data for cubic La$_{0.6}$Sr$_{0.1}$TiO$_3$ are those of the quenched sample collected at temperatures above $\sim$570 K. They are not of sufficient quality to allow a fit of Eq. (21) with Θ_{s0} as a free parameter, however. For SrTiO$_3$ it has been found[17] that Θ_{s0} is $\sim$130 K, while for LaAlO$_3$ and (La, Pr)AlO$_3$, Θ_{s0} values are $\sim$250 and $\sim$300 K, respectively.[27,29] For present purposes Θ_{s0} = 250 K has been fixed arbitrarily in order to obtain some estimates of the volume strain e_a. The fit for a_0 in Fig. 4 was obtained for data from the quenched sample collected in the range 573–773 K and has $a_1 = 3.8679$ Å and a_2 = 0.000 039 76 Å K^{-1} (Θ_{s0} = 250 K). This was then used in calculations of e_1, e_2, and e_3 and, hence, of the symmetry-adapted strains shown in Fig. 6. Shear strains (e_t, e_o) are relatively insensitive to the choice of a_0 values.

The slowly cooled sample has effectively constant values of e_t and e_a in the temperature range 573–773 K. This is consistent with the expectation that the degree of cation order (q_2) remains constant in this temperature interval over the time scale of data collection. The onset of octahedral tilting is clearly indicated by the development of an orthorhombic strain and a change in the trend of the tetragonal strain near 570 K. Also as expected, e_o scales linearly with ϕ^2 [Fig. 7(a)], consistent with Eq. (8), and e_o^2 scales linearly with temperature [Fig. 7(b)], consistent with the tricritical character suggested by Fig. 5(b). The straight line fit in Fig.

7(b) gives a $P4/mmm \leftrightarrow Cmmm$ transition temperature (T_{c2}^*) of 560 K. Changes in e_a and e_t due to this transition are given by the difference between observed values for the $Cmmm$ structure and constant values for the $P4/mmm$ structure. The latter have been obtained by averaging data collected in the temperature range 673–773 K (Fig. 6) and lead to the variations of e_a and e_t associated only with the tilting transition shown in Fig. 7(c). When analyzed in this way, there is a small tail in e_t above T_{c2}^* that implies the existence of precursor effects ahead of the transition point. While e_t behaves in a regular and predictable manner in relation to coupling with the order parameter, e_a apparently does not. The volume strain perhaps only starts to develop $\sim$50 K below T_{c2}^* and then deviates substantially from the expected trend below $\sim$450 K. The precise values of e_a are highly sensitive to the choice of a_0 but a similar reversal in the trend of e_a with falling temperature has also been observed in (Ca, Sr)TiO$_3$ (Refs. 28 and 30) and NaMgF$_3$ (Refs. 31 and 32) perovskites. Equations (7) and (8) require that $e_t\sqrt{3}$ = $-e_o$, where e_t is now the tetragonal strain due to $P4/mmm \leftrightarrow Cmmm$ alone, and this is indeed obtained [Fig. 7(d)].

Lattice parameters for the sample quenched from high temperature show quite different patterns of evolution from
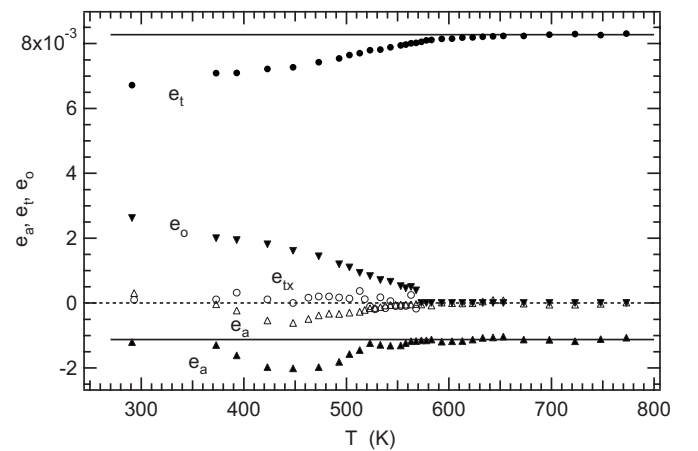
FIG. 6. Symmetry-adapted strains calculated from the lattice parameter data given in Fig. 4. Filled symbols represent results for the slowly cooled sample and open symbols represent results for the quenched sample. Horizontal lines represent constant values of e_t and e_a for the $P4/mmm$ structure, as determined by averaging data from the range 673–773 K.
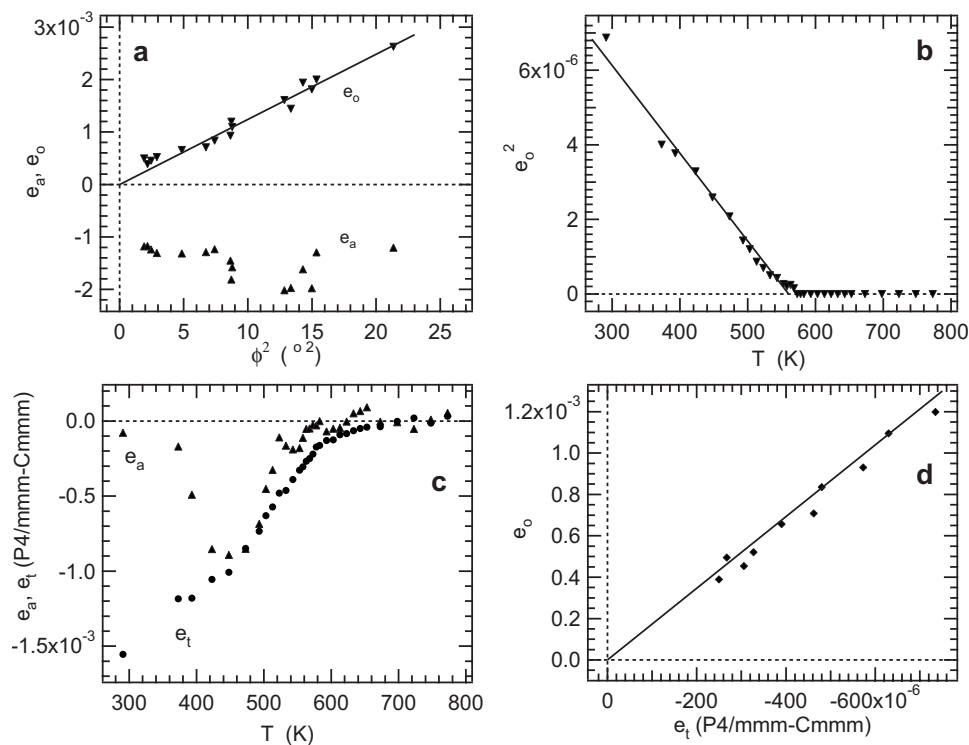
FIG. 7. Strain relationships for the slowly cooled sample. (a) e_o varies linearly with the square of the octahedral tilt angle ϕ. (b) The square of the orthorhombic strain varies linearly with temperature, consistent with tricritical character for the octahedral tilting transition $[q_5^4 \propto (T_{c2}^* - T)]$. (c) Tetragonal strain e_t and volume strain e_a for the $P4/mmm \leftrightarrow Cmmm$ transition, as obtained by subtracting contributions due to cation ordering $(Pm\bar{3}m \leftrightarrow P4/mmm)$ from the total strain. (d) Orthorhombic strain and tetragonal strain for the $P4/mmm \leftrightarrow Cmmm$ transition are related by $e_t\sqrt{3} = -e_o$ (solid line).

those of the slowly cooled sample (Fig. 4). The $Pm\bar{3}m \leftrightarrow I4/mcm$ transition occurs near 570 K, as shown by the evolution of the tilt angle (Fig. 5), but the tetragonal distortion is barely detected. At $e_t, e_a < 0.001$, the strains calculated from these data are close to the instrumental limit of resolution, and details of their evolution probably do not merit close analysis. It is notable, however, that both the magnitude and pattern of evolution of e_a (Fig. 6) are very similar to those shown by the $P4/mmm \leftrightarrow Cmmm$ transition [Fig. 7(c)]. Octahedral tilting is not substantially modified by disordering of the cations in La$_{0.6}$Sr$_{0.1}$TiO$_3$, but coupling of the order parameter to the shear strain e_t appears to be almost entirely suppressed.

DISCUSSION

In La$_{0.6}$Sr$_{0.1}$TiO$_3$, one of the order parameters operates on a time scale that is determined by the rate of diffusion of cations between A sites of the perovskite structure, while the second responds rapidly to changes in temperature. The coupling is biquadratic and is thus analogous to the combination of Al/Si ordering and a displacive transition in the mineral anorthite, CaAl$_2$Si$_2$O$_8$, as described in several publications elsewhere.[5,6,33–35] A standard Landau description [Eq. (1)], combined with an understanding of these different time scales, leads to predicted behavior which appears to be broadly correct. The transition temperature of the tilting tran-

sition, T_{c2}^*, is only weakly dependent on the degree of cation ordering in that a difference of ~ 10 K was found between the quenched and slowly cooled samples [Fig. 5(b)]. However, the strength of coupling between octahedral tilting and the shear strain appears to be highly sensitive to the degree of cation order, and there is perhaps also a small difference in the evolution of q_5 below T_{c2}^* in that the slopes of ϕ^4 against T are slightly different for the two samples [Fig. 5(b)]. This is contrary to the expectation from Eq. (5) that the coefficients b_2^* and $c_2 + c_2''$ remain the same for both cases [Eqs. (10)–(12)]. The implication is that the coupling coefficient λ_4 might itself be explicitly dependent on q_2. In the lowest order permitted by symmetry, λ_4 could be replaced by $\lambda_4' q_2^2$, such that $\lambda_4 = 0$ when $q_2 = 0$. A term of the form $\lambda_4' e_t q_2^2 q_5^2$ then appears in Eq. (5), with interesting consequences for unusual variations of e_t in crystals investigated under time-temperature conditions which allow simultaneous equilibration of both cation ordering and octahedral tilting. It follows from replacing λ_4 by $\lambda_4' q_2^2$ that b_2^* is also sensitive to cation disordering [Eq. (12)], and the precise evolution of the octahedral tilt angle will then also be different in crystals with different degrees of order.

It has previously been found that strain–order-parameter coupling can be suppressed in (Ca,Sr)TiO$_3$ perovskites while octahedral tilting is hardly affected.[28] This effect was explained as being due to the development of local (unit cell scale) strain heterogeneities caused by lattice relaxations around Ca substituted for Sr and around Sr substituted for

Ca. The local strain fields were construed to act in such a way that the development of a coherent, long-ranging relaxation due to the tilting transition becomes frustrated. More direct evidence for the existence of local strain heterogeneities in perovskites is provided by line broadening in infrared absorption spectra,[36] while in silicates the heterogeneities appear to be eliminated by cation ordering.[37–43] It is therefore proposed that similar local strain fields are induced by cation disordering in $La_{0.6}Sr_{0.1}TiO_3$, and that it is these local heterogeneities which are responsible for the suppression of strain–order-parameter coupling. A slight increase in the widths of superlattice reflections from the disordered sample, relative to those from the ordered sample, suggests smaller antiphase domain sizes and may imply that domain growth is also hindered by the disordering.

The influence of cation disordering appears to be quite different between ferroelastic and ferroelectric materials. Rather than retaining a discrete transition as in the ferroelastic case considered here, cation disorder can cause smearing of a ferroelectric transition.[8–10] It is likely that there are equivalent local strain relaxations in the ferroelectric material but these appear to give rise to regions of crystal with different transition temperatures. Potential applications of the strain–order-parameter suppression mechanism in ferroelastic materials might involve predetermination of the properties of twin walls. For example, ferroelastic switching involves transformation of one twin orientation to another. If the spontaneous strain associated with each twin can be reduced to a negligible value by the choice of chemical composition and state of cation disorder, the stresses accompanying switching might be substantially lowered. Alternatively, if the requirement is to have a high resistance to switching in some multiferroic material, the choice of an ordered material with large strains might be more appropriate.

[1] W. Eerenstein, N. D. Mathur, and J. F. Scott, Nature (London) **442**, 759 (2006).

[2] S.-W. Cheong and M. Mostovoy, Nat. Mater. **6**, 13 (2007).

[3] E. K. H. Salje, Phys. Chem. Miner. **12**, 93 (1985).

[4] E. K. H. Salje, B. Kuscholke, B. Wruck, and H. Kroll, Phys. Chem. Miner. **12**, 99 (1985).

[5] E. K. H. Salje, Phys. Chem. Miner. **14**, 181 (1987).

[6] S. A. T. Redfern, Phys. Chem. Miner. **19**, 246 (1992).

[7] S. A. T. Redfern, Phase Transitions **55**, 139 (1995).

[8] N. Setter and L. E. Cross, J. Appl. Phys. **51**, 4356 (1980).

[9] N. Setter and L. E. Cross, J. Mater. Sci. **15**, 2478 (1980).

[10] C. Zhili, N. Setter, and L. E. Cross, Ferroelectrics **37**, 619 (1981).

[11] C. J. Howard and Z. Zhang, J. Phys.: Condens. Matter **15**, 4543 (2003).

[12] C. J. Howard and Z. Zhang, Acta Crystallogr., Sect. B: Struct. Sci. **60**, 249 (2004); **60**, 763(E) (2004).

[13] C. J. Howard, G. R. Lumpkin, R. I. Smith, and Z. Zhang, J. Solid State Chem. **177**, 2726 (2004).

[14] The irreps here are written using the notation of S. C. Miller and W. F. Love, *Tables of Irreducible Representations of Space Groups and Co-representations of Magnetic Space Groups* (Pruett Press, Boulder, CO, 1967).

[15] C. J. Howard and H. T. Stokes, Acta Crystallogr., Sect. A: Found. Crystallogr. **61**, 93 (2005).

[16] H. T. Stokes and D. M. Hatch, computer code ISOTROPY (Brigham Young University, Salt Lake City, Utah, 2002), http://www.physics.byu.edu/~stokesh/isotropy.html

[17] M. A. Carpenter, Am. Mineral. **92**, 309 (2007).

[18] A. E. Ringwood, S. E. Kesson, K. D. Reeve, D. M. Levins, and E. J. Ramm, in *Radioactive Waste Forms for the Future*, edited by W. Lutze and R. C. Ewing (Elsevier, Amsterdam, 1988), pp. 233–334.

[19] R. M. Ibberson, W. I. F. David, and K. S. Knight, Rutherford Appleton Laboratory Report No. RAL92-031, 1992 (unpublished).

[20] H. M. Rietveld, J. Appl. Crystallogr. **2**, 65 (1969).

[21] A. C. Larson and R. B. von Dreele, Los Alamos National Laboratory Report No. LAUR 86-748, 2000 (unpublished).

[22] B. H. Toby, J. Appl. Crystallogr. **34**, 210 (2001).

[23] B. S. Thomas, N. A. Marks, and P. Harrowell, Phys. Rev. B **74**, 214109 (2006).

[24] Z. Zhang, G. R. Lumpkin, C. J. Howard, K. S. Knight, K. R. Whittle, and K. Osaka, J. Solid State Chem. **180**, 1083 (2007).

[25] E. K. H. Salje, B. Wruck, and H. Thomas, Z. Phys. B: Condens. Matter **82**, 399 (1991).

[26] E. K. H. Salje, B. Wruck, and S. Marais, Ferroelectrics **124**, 185 (1991).

[27] M. A. Carpenter, C. J. Howard, B. J. Kennedy, and K. S. Knight, Phys. Rev. B **72**, 024118 (2005).

[28] M. A. Carpenter, C. J. Howard, K. S. Knight, and Z. Zhang, J. Phys.: Condens. Matter **18**, 10725 (2006).

[29] S. A. Hayward, S. A. T. Redfern, and E. K. H. Salje, J. Phys.: Condens. Matter **14**, 10131 (2002).

[30] M. A. Carpenter, A. I. Becerro, and F. Seifert, Am. Mineral. **86**, 348 (2001).

[31] M. A. Carpenter, E. K. H. Salje, and A. Graeme-Barber, Eur. J. Mineral. **10**, 621 (1998).

[32] M. A. Carpenter, Rev. Mineral. Geochem. **39**, 35 (2000).

[33] S. A. T. Redfern and E. K. H. Salje, Phys. Chem. Miner. **14**, 189 (1987).

[34] S. A. T. Redfern, A. Graeme-Barber, and E. K. H. Salje, Phys. Chem. Miner. **16**, 157 (1988).

[35] R. J. Angel, Am. Mineral. **77**, 923 (1992).

[36] H. W. Meyer, M. A. Carpenter, A. I. Becerro, and F. Seifert, Am.

Mineral. **87**, 1291 (2002).

[37] T. Boffa Ballaran, M. A. Carpenter, M. C. Domeneghetti, E. K. H. Salje, and V. Tazzoli, Am. Mineral. **83**, 434 (1998).

[38] A. J. Atkinson, M. A. Carpenter, and E. K. H. Salje, Eur. J. Mineral. **11**, 7 (1999).

[39] M. A. Carpenter, T. Boffa Ballaran, and A. J. Atkinson, Phase Transitions **69**, 95 (1999).

[40] E. K. H. Salje, M. A. Carpenter, T. Malcherek, and T. Boffa Ballaran, Eur. J. Mineral. **12**, 503 (2000).

[41] M. A. Carpenter and T. Boffa Ballaran, Eur. Mineral. Union Notes Mineral. **3**, 155 (2001).

[42] M. A. Carpenter, Eur. Mineral. Union Notes Mineral. **4**, 311 (2002).

[43] S. C. Tarantino, T. Boffa Ballaran, M. A. Carpenter, M. C. Domeneghetti, and V. Tazzoli, Eur. J. Mineral. **14**, 537 (2002).